International Journal of Ecology & Development
Special Issue on the Coastal Environment, 2007

Wave Climate Hindcast for the Design of Offshore Wind Energy Structures in the German Bight

K. Mittendorf[1], B. Sweetman[1] and W. Zielke[2]

[1]Maritime Systems Engineering Department, Texas A&M

200 Seawolf Parkway, Galveston, Texas 77553, USA

mittendk@tamug.edu

[2]Institute of Fluid Mechanics and Computer Applications in Civil Engineering

Leibniz Universität Hannover

Appelstraße 9A, 30167 Hannover, Germany

ABSTRACT

Design of offshore wind turbines against ultimate limit state requires estimation of the most severe wave loading expected during the life of the wind turbine. Measured wind and wave data spanning sufficient duration to statistically predict these maximum loads are generally not available for most areas considered for wind farm development. One method used to develop the necessary design criteria is numerical simulation of environmental conditions at an offshore development site. Here, the effectiveness of the simulation methodology is assessed by critical comparison between design values based on simulated environmental conditions and equivalent design values based on measured buoy data. Specifically, the wind-wave activity in the German Bight is simulated for a twelve-year period using WaveWatch-III and SWAN. The simulation results are used to predict the significant wave height, the fifty-year mean-maximum wave height, and the fifty-year mean-maximum wave loading on a turbine support structure. Extreme values of significant wave heights are generally observed to be overpredicted compared with the hindcast methodology. In the load and response calculation the influence of the associated wave period is found to have a greater effect than this relatively small overprediciton of wave heights.

Keywords: significant wave height, hindcast, extreme wave, design condition, wave loads, offshore wind turbines.

Mathematics Subject Classification:

1 Introduction

Offshore wind energy can only become economical if adequate design methods allow highly optimized and robust structures with a long lifespan. The move from land to sea requires significant changes in the design methodologies relevant to wind energy

converters. The new methodologies must rationally account for not only the complex wind loading environment, but also the equally complex wave loading. A reliable and optimized design process for an offshore wind energy converter (OWEC) requires detailed knowledge of the wave environment over the lifetime of the structure. This detailed knowledge must include both determination of extreme events and characterization of the normal operating conditions.

Measured wave data, if available, are often sparse for the specific locations necessary for effective offshore wind farm planning. One alternative is to estimate wave conditions by application of physical principles for wave generation and decay (World Meteorological Organization, 1988) in conjunction with wind information from measurements and/or meteorological models. Numerical models like SWAN or WAM are design tools conventionally used in this wave-simulation process.

Here, the typical wave simulation process is tested against measured wave data. A numerical hindcast based on measured wind records covering the twelve-year period from 1989 to 2000 and has been performed for the German Bight. The analysis includes a non-stationary simulation using phase averaging wave models WaveWatch-III (Tolman, 1999) and SWAN (Holthuijsen, 2000). Wavewatch is used on a relatively course gird to generate far-field wave conditions which become boundary conditions for a local SWAN model on a much finer grid. The regional SWAN model is forced by initial conditions from the global scale WaveWatch-III model. Those global models ensure optimal turnaround times, but may not be suitable for capturing the physics of the shallow water environment. Thus, nesting of WaveWatch-III results enables more accurate predictions for shallow water depths. Results have been statistically analyzed with regard to operational and extreme conditions. An overview of the numerical coupling procedure is illustrated in Figure 1.

2 Model of the European Shelf

Ocean waves are a combination of swell generated by winds far from the field site and locally generated wind-driven waves. A compromise between accuracy and model dimension has to be found for each sea state simulation. Some geographic areas, such as the European Continental Shelf, have relatively little swell traveling into the region. For such areas, large models can be assumed to be closed because the influence of swell is negligible compared with that of locally wind-driven waves.

The model of the European Shelf (Figure 2) complies with these requirements. The computational grid has a resolution of 51 times 44 nodes and covers the region from 12°W to 13°E (Δx=0.5° or about 32km) and from 48° N to 62° N (Δy=0.3° or about 33km at 50°). The WaveWatch-III code was used to simulate the sea state in the Shelf model. The hindcast wind fields driving the model are from the synoptic PRISMA model (interpolation model for measured wind data) of the Max Planck Institute for Meteorology (Luthardt, 1987). The computational time step for the model run was 15 minutes and wind fields were updated every 3 hours. PRISMA wind fields are based on observations from ships and from measurement stations close to the coast.

3 Model of the German Bight

Near-shore areas typically proposed for wind-farm development are often influenced by finite-depth effects including bottom friction, shoaling, refraction, depth-induced wave breaking, and wave-wave interaction. These important near-shore effects have been included in the numerical SWAN model of the German Bight.

The SWAN model requires use of a computational grid that is much finer than that of WaveWatch-III. The model covers the area between 5.9° E to 9.2° E and 53.2° N to

55.5° N with a resolution of 200 times 200 nodes or about 1 km square grid (Figure 3). The input winds are also those from the PRISMA model. On the open boundaries, spectra simulated using WaveWatch-III have been used. The nesting is illustrated in Figure 4. To validate the model of the German Bight, the computed wave parameters have been also compared with buoy measurements.

4. Comparison of Simulated and Measured Significant Wave Heights

4.1 Measured Field Data

Extensive measurements taken at the North Sea Buoy II are used for comparison with the two hindcast models presented. This data was collected in the German Bight as part of the "Bundesamt für Seeschiffahrt und Hydrographie (BSH)" (Mittendorf, K. and Zielke, W., 2004). The buoy is located in 42 m deep water at the location shown in Figure 3. Data was collected over the period from August 1993 to February 2005 with only small gaps in the observational data. Each field data point (significant wave height, H_s and peak period T_p) is assumed to represent a stationary process for a 3-hour duration, which implies a total of 2920 sea state observations per year. Every three hours, one 20-minute sample of the water surface elevation has been taken which is used to calculate the wave spectrum and to estimate H_s and T_p.

Numerical hindcasting has been performed using each of the two models, Wavewatch and SWAN, covering the years 1989 to 2000. Consistent with the field data, each significant wave height resulting from a hindcast prediction is assumed to represent a 3-hour stationary process.

4.1 Methodology

First, differences between model predictions and field measurements of significant wave heights are investigated. Significant wave heights, H_s, are divided into constant classes of ΔH_s =1.0m, starting with class 1 from 0.5m to 1.5m. The number of occurrences of 3-hour sea states having significant wave heights within each bin are counted. The bins are then normalized by the total number of observations such that the histogram can be treated as a probability distribution.

After this broad comparison between predicted and observed significant wave heights, the implications of these predictions in terms of likelihood of extreme wave heights and loading on a wind-turbine support structure are investigated in Sections 5 and 6, respectively.

4.2 Results: North Sea Buoy II

In general, a good agreement between the time history of modeled and measured significant wave heights, H_s, has been observed for the location of the North Sea Buoy II (NSB-II). Figures 5 and 6 compare the time histories of significant wave height as a function of time for the years 1997 and 2000, and present the probabilistic cumulative density functions (CDF's) of significant wave height.

Comparison of the CDF's shows reasonably good agreement for relatively large values of H_s, which are the values of interest for practical engineering considerations such as maximum load. The CDF's also show that significant wave heights in the medium range ($1.5m \leq H_s < 4.5m$) have been systematically underestimated and that the occurrence of lower significant wave heights ($H_s < 1.5m$) have been overestimated.

Figure 7 compares the relative frequency of occurrence of significant wave heights as predicted by SWAN and WaveWatch-III. The bars represent mean values of the significant wave heights, which consistently underpredict the actual field measurements. Figure 8 compares annual means of the significant wave heights. Results from the SWAN model are closer to the measured field data than the WaveWatch-III model, but still underpredict in each of the eight years. From a practical design standpoint, the more extreme (larger) sea states are of considerably more interest than are the averages presented here.

Figure 9 shows a scatter plot of measured and simulated data. Each data point represents an observed or predicted 3-hour significant wave height. A strong linear relationship is observed between the measured and predicted values with relatively minor scatter. The linear regression curve differs from the (45 degree) line of equality, with a slope of 37 degrees, which indicates an almost linear deviation of the simulated wave heights from the measurements, with the Wavewatch model underpredicting field measurements by an average of 17.5%. The scatter index (ratio of standard deviation of difference to mean of measurements) is 19%.

Figure 10 shows an empirical quantile-quantile plot (EQQ) of significant wave heights from buoy measurements and from numerical simulations with WaveWatch-III during 1989 through 2000. Each point on the EQQ plot represents the same percentile for the Wavewatch prediction as for the measured data, e.g., the point farthest up and to the right represents the 0.9998-percentile of each distribution. Two data sets with equivalent underlying distributions will exhibit these points scattered around the line $y = x$.

Interestingly, Figure 10 shows that the Wavewatch model significantly overpredicts the field measurements for the extreme values (by approximately 10%). These overpredictions of extreme-values are in direct contrast to the average predictions

presented earlier: while the Wavewatch model generally underpredicts significant wave hights, it overpredicts the extreme values of greatest interest for practical design purposes. Extreme value predictions are investigated more fully in Section 5.

Figure 11 presents an equivalent EQQ plot for the SWAN predictions. Comparing Figures 10 and 11, SWAN generally overpredicts for more of the data than Wavewatch, but the SWAN model shows a more linear trend in the predictions, and does not exhibit the marked departure from the measured data for extreme values noted for Wavewatch.

Considering all of the data (comparison of point-to-point values), differences between hindcast and buoy measurement have ranged between 5% and 36%, with the hindcast models generally overpredicting measured buoy data. De Valk et al. (2004) also observed hindcast data to overestimate measured conditions.

5 Extreme Value Analysis

5.1 Methodology

The Weibull extreme-value distribution is used to predict significant wave heights, H_S, with return periods 1, 5, 10, 20, 50 and 100 years. The extensive list of return periods is in keeping with the DNV guidelines DNV-OS-J101 (2004). Applicability of this distribution is confirmed through visual inspection of the complete data plotted on a Weibull scale (Figure 12 and Figure 13). Data points falling on a straight line indicate a Weibull distribution is appropriate.

The 2-parameter Weibull distribution is defined by its cumulative distribution function (CDF):

$$F_{H_S}(x) = 1 - \exp\left(-\left(\frac{x}{a}\right)^c\right) \tag{5.1}$$

in which *a* is a scale parameter and *c* is a shape parameter. These parameters are fit from the data using the method of maximum likelihood estimation (mle).

The Weibull distribution is used to predict the extreme sea state (the long-term problem). Once the extreme sea state has been defined, the Rayleigh distribution is used to predict the most extreme wave expected during a 3-hour realization of that sea state (the short-term problem). The Rayleigh distribution is commonly used to predict extreme values of individual wave heights for offshore wind turbines (e.g. Germanischer Lloyd, 2005 or DNV, 2004)

$$F(H) = 1 - \exp\left(-\frac{H^2}{H_S^2}\right). \tag{5.2}$$

The largest wave height H_{max} expected in N waves is given by

$$\frac{H_{\max}}{H_S} = \frac{\sqrt{2}}{2}\sqrt{\ln\left|\frac{N}{\ln(1/(1-\mu))}\right|}. \tag{5.3}$$

in which μ is the probability of exceedence (Goda, 2000) and is set here to μ = 0.57.

An estimate of the zero-downcrossing or zero-upcrossing wave period, T_z, for the seastate when the significant wave height has an extreme value is obtained by assuming a specific value for the significant wave steepness (WMO, 1998, Goda, 2000 or Battjes, 1979).

The WMO (1998) suggests the following relation:

$$\frac{2\pi \cdot H_s}{g \cdot T_z^2} = 0.055556 \tag{5.4}$$

gravitation: g

significant wave height: H_S

wave period: T_z.

Goda (2000) gives:

$$\frac{2\pi \cdot H_s}{g \cdot T_z^2} = 0.04 \; to \; 0.03 \tag{5.5}$$

Battjes (1979), assuming a maximum wave steepness, proposes the following formula:

$$T_z = \left(\frac{32 \cdot \pi \cdot H_S}{g} \right)^{0.5} \tag{5.6}$$

These formulas can be applied to obtain a range for the associated mean zero-crossing wave periods. Here, wave periods and water surface elevations have not been preserved. The corresponding design wave periods T_{Hmax} given in Table 4 have been estimated using the determined mean zero-crossing wave period calculated from the wave spectrum and the following relationship given by Goda (2000):

$$T_{Hmax} = 0.6.T_{Hs} \text{ to } 1.3.T_{Hs}. \tag{5.7}$$

T_{Hmax}: period of max. wave in the record

T_{Hs}: mean wave period of the highest one-third of all waves (zero-downcrossing)

5.2 Results

The regression analysis of the complete significant wave heights based on maximum likelihood estimation (mle) has led to the Weibull distribution parameters given in Table 1. The corresponding distribution functions plotted on Weibull scale are given in Figure 12 (measured wave heights) and in Figure 13 (simulated).

In the next analysis, only the annual maximum values of the significant wave heights are considered, these maxima are fit to a Weibull distribution (Table 2).

The significant wave height with a desired return period T_R has been defined as the $(1\text{-}1/T_R)$-quantile in the distribution of annual maximum significant wave heights.

The results for the NSB-II data sets are given in Table 3. The wave heights based on the annual maximum series have been used. The differences between extrapolated extreme significant wave heights vary between 8.0% and 6.3%. The absolute deviation between hindcast and measurement stays nearly constant for all considered return periods.

The 50-year significant and individual design wave heights have been calculated from the cumulative data fit with the Weibull distribution and are given in Table 4. The extrapolation of the numerical hindcast data set results in a 50-year extreme (design) wave which is about 9% higher than the one derived from the buoy measurement (Table 4).

6 Extreme Load Analysis

In this section, the effect of the extreme wave height on the total load on an offshore wind turbine support structure is analyzed. Calculations are based on the extrapolated individual extreme waves from hindcast and buoy data. No relationship for a maximum individual wave height and its associated wave period has been theoretically confirmed. Thus, the simulations have been carried out with four different wave periods (Table 6), in accordance with the recommended load effect analysis of the DNV guidelines DNV-OS-J101 (2004).

Wave loads have been determined using the Morison equation. The wave kinematics have been calculated with 7^{th} order regular Fourier wave model in formulation by Sobey (1989) and the hydrodynamic coefficients have been constant per DNV (C_d=2.0 and C_m=0.7).

The dimensions of the monopile model with tapering diameter (decrease from bottom to top) and restrained abutment in 30m water depth are given in Table 5 and Figure 15. The first natural frequency of the structure is 0.266Hz, which is in accordance with typical observed natural frequencies of existing monopole turbines ranging from 0.18 Hz to 0.35 Hz (Kühn, 2001).

Load predictions using the shortest wave (B1) and using the longest (H4) result in the highest total load. However, when structural dynamics are included in the analysis (Section 7), that longest wave (H4) does not result in the highest predicted response. The range of periods has involved a variation in the total loads up to 8%. An increase of the wave height from 14.0m to 15.26m (9%) has given rise to a total load increase of 5% to 14%, depending on chosen wave period (Figure 14 and Table 6).

7 Extreme Response Analysis

Finally, the effect of varying the design wave height on the structural response is investigated considering maximum horizontal force in the abutment of the support structure. A three dimensional finite element analysis is used for the response calculation in which the equation of motion is solved in the time domain using the Newmark integration scheme within the commercial ANSYS package.

Table 6 summarizes the response amplitudes predicted using the design wave approach, in which only a single extreme wave is considered. The results show the maximum response strongly depends on wave period. In addition to the previously observed dependence in the loads, here the ratio between the response and the load varies considerably. This variation demonstrates the influence of structural dynamics on the maximum response. The dynamic amplification variation between 0.5% and 21% indicates that the response should be investigated using a spectral analysis rather than

the design wave approach. However, the strong nonlinearities inherent to the Morrison equation require that force-predictions be carried out in the time-domain.
Here, a mixed analysis is applied. Time histories of the sea surface are realized from a spectral representation of the sea state; forces and structural response resulting from these time histories are predicted using the Morrison equation and an ANSYS model, and a power-spectrum is computed from the time-history of the response.

Two of these mixed analyses have been performed. The first applies a design sea state based on the extreme values of significant wave height, H_s, resulting from measured buoy data (H_s=7.46m, T_p=11.20s); the second uses a design sea state based on the hindcast data (H_s=8.21m, T_p=12.70s).

In each case, the extreme sea state condition is characterized by a JONSWAP wave spectrum, which is used to simulate an irregular time history of water surface elevation and the associated kinematics using Stokes' first-order (Airy) theory. The response power-spectrum has been computed as the squared amplitude of the Fourier spectrum of the response time history. The area under a power spectrum equals the variance of the process and is proportional to the total energy of the system.

Figure 16 shows the calculated wave spectra, load amplitude spectra, and response spectra for each of the extreme sea states based on buoy data (H_s=7.46m, T_p=11.20s) and on hind-cast data (H_s=8.21m, T_p=12.70s). As would be expected, the peaks of each load spectrum occur at frequencies identical with those of the input wave spectra. Similarly, the area under the load spectrum 1 (H_s=7.46m, T_p=11.20s), is smaller than the area of load spectrum 2 (H_s=8.21m, T_p=12.70s), i.e., the larger sea state results in larger loads.

The shapes of the response spectra, however, diverge from those of the wave and force spectra because of dynamic effects of the structure. Most notably, there is significant energy observed near the natural frequency of the structure, which appears as a hump in the high frequency regions. Also, the response resulting from the smaller wave and force spectra are larger than those resulting from the larger spectra: about 14% larger. This change is caused by structural dynamics effects which are dominating the high-frequency part of the response.

The maximum expected structural response, here the maximum horizontal force in the abutment, is a critical design quantity. To predict this design value, the sea state is assumed stationary for a period of three hours. In general, any single observed maximum associated with a storm condition is not a robust estimator of the expected maximum for that sea state. Part of the irregular simulation process is random selection of phase angles, and an observed maximum in any irregular simulation depends strongly on these phase angles. A much more robust estimation of the maximum response can be obtained directly from the spectrum. Assuming the process is Gaussian, the mean maximum of the response amplitude, R, can be estimated as (e.g. Madsen et al., 1986, from Cartwright & Longuet-Higgins, 1956):

$$E[\max R] = \left[\sqrt{2\ln(N)} + \frac{0.577}{\sqrt{2\ln(N)}}\right] \cdot \sigma_R \qquad (7.1)$$

N: number of cycles

σ: standard deviation

Table 7 presents mean maxima of the response amplitudes for a 3-hour storm event. The predicted extreme response for the lower sea state is about 11% higher than that of the higher sea state. This increase in maximum response is directly attributable to the

peak frequency of the smaller sea state's being nearer to the natural frequency of the structure.

8 Summary and Conclusion

Design wave parameters for an offshore wind energy turbine in the German Bight have been determined from two interrelated numerical simulation models and from buoy measurements. For the simulation approach, models of the European Shelf and the German Bight have been coupled. A hindcast over a twelve-year period has been performed based on historical wind measurements. The accuracy of the simulation results has been assessed by critical comparison with measured buoy data. The comparison of measurements and model output for different times and locations has shown reasonable agreement (deviations less than 10%), with the simulation model tending to over predict the significant wave heights for the larger sea states which are more interesting for design purposes.

For one location in the German Bight (NSB-II), distributions of maximum significant wave heights have been determined from both hindcast modeling and buoy data. Hindcast-predicted significant wave heights are about 6% to 8% higher than those predicted by the buoy data for equivalent return periods (Figures 5 and 6).

Sea states associated with each of these extreme significant wave heights, $H_{s,}$ are then used with a Rayleigh distribution to predict the highest individual wave, H, generally regarded as the design wave. The combination of wave height and period causing the highest load on the structure is considered as the design case.
The DNV recommendation of analyzing structural response for a range for valid wave periods is applied, in addition to empirically-based relationships between wave height and period. Here, the empirical relationship between wave height and wave period,

found by Goda (2000) has been used to derive a range of wave periods associated with the determined design wave heights. A change of the wave period associated with a constant wave height results in a variation of the wave load of about 8% (Table 6). Whereas, an increase of 9% in the design wave height from 14.0m (buoy data) to 15.26m (hindcast data) increases the total load by only 5% to 14%, depending on wave period. The wave period is observed to have a strong influence on maximum horizontal force in the abutment of the support structure. The ratio between the response and the load varies considerably. The dynamic amplification variation between 0.5% and 21% indicates the necessity of using a spectral analysis rather than the design wave approach. Strong nonlinearities inherent to the Morrison equation require that the force-predictions have been carried out in the time-domain and the response power-spectrum has been computed by Fourier transformation from the response time history. For the two investigated cases (Figure 16), the peak period was found to have a larger effect on the maximum structural response than the significant wave height. A robust estimation method published by Madsen et al. (1986) has been used for the determination of the maximum response from the spectrum. The response resulting from the 9% lower sea state is larger than those resulting from the larger one: about 11% increase in maximum response amplitude. This change is caused by structural dynamics effects which are dominating the high-frequency part of the response and underlines the strong influence of the wave period on the maximum response.

Overall, the numerical wave hindcast resulted in reasonable accuracy for the prediction of design wave parameters with some small inherent conservatism. Use of the more accurate in situ measurements, where available, would be expected to allow a slightly less robust and therefore less expensive structural design.

REFERENCES

Battjes, J.A., 1970, *A long-term Wave Height Distribution at Seven Stations around the British Isles*, N.I.O. Report A44.

Cartwright, D. E. and Longuet-Higgins, M. S., 1956. *The statistical distribution of the maxima of a random function*, Proc. Roy. Soc. London, Ser. 76, 5002.

de Valk, C., Groenewoud, P., Hulst, S., and Klopman, G., 2004, *Building a global Resource for Rapid Assessment of the Wave Climate*, Proceeding of the 23rd International Conference on Offshore Mechanics and Arctic Engineering (OMAE), 1–9.

Det Norske Veritas (DNV), 2004, *Offshore Standard DNV-OS-J101, Design of Offshore Wind Turbine Structures*, Offshore Standard DNV-OS-J101, Det Norske Veritas.

Forristall, G., 1978, *On the Statistical Distribution of Wave Height in a Storm*, Journal of Geophysical Research, Vol. 83, 2353-2358.

Germanischer Lloyd, 2005, Guideline for the Certification of Offshore Wind Turbines, Edition 2005.

Goda, Y., 2000, *Random Seas and Design of Maritime Structures*, Advanced Series on Ocean Engineering, Volume 15, World Scientific Publishing Company.

Holthuijsen, L., N. Booij, R. Ris, I. G. Haagsma, A. Kieftenburg, E. E., Kriezi, 2000, *SWAN Cycle III Version 40.11 - User Manual*, Delft University of Technology Department of Civil Engineering, Netherlands.

Kühn, M., 2001, *Dynamics and Design Optimisation of Offshore Wind Energy Conversion Systems,* Doctoral Thesis, DUWIND Wind Energy Research Institute TU Delft, Netherlands.

Luthardt, H., 1987, *Analyse der wassernahen Druck- und Windfelder über der Nordsee aus Routinebeobachtungen*, Hamburger Geophysikalische Einzelschriften, Reihe A 83, Fachbereich Geowissenschaften, Universität Hamburg, Deutschland.

Madsen, H.O., Krenk, S., Lind, N.C., 1986, Methods of Structural Safety, Prentice-Hall, Englewood Cliffs.

Mittendorf, K., 2006, *Hydromechanical Design Parameters and Design Loads for Offshore Wind Energy Converters*, Doctoral Thesis, Leibniz University of Hannover, Germany.

Mittendorf, K. and Zielke, W., 2004, *A Hindcast Data Base for the Design of Offshore Wind Energy Strucutres in the German Bight*, Proceedings 29th International Conference on Coastal Engineering (ICCE), Lisbon, 2004.

Tolman, H., 1999, *User Manual and System Documentation of Wave-Watch-III Version 1.18*, U.S. Department of Commerce, National Oceanic and Atmospheric Administration, National Weather Service, National Centre for Environmental Prediction.

Sobey, R. J., 1989, *Variations on Fourier Wave Theory*, International Journal for Numerical Methods in Fluids, 9, 1453–1467.

World Meteorological Organization (WMO), 1988, *Guide to Wave Analysis and Forecasting*, WMO-Report No. 702, Genf.

TABLES

Data Set Info	Scale Parameter a	Shape Parameter c
Buoy	2.0207	1.6914
Hindcast	1.8126	1.3184

Table 1 Weibull Parameters fit for NSB-II.

Data Set Info	Scale Parameter a	Shape Parameter c
Buoy	8.4984	10.4458
Hindcast	9.1693	116436

Table 2 Weibull Parameters fit for NSB-II Annual Maximum Series.

Return Period [year]	H_s [m] Buoy	H_s [m] Hindcast	Difference [m]	Difference [%]
1	8.49	9.17	0.68	8.01
5	8.89	9.55	0.66	7.42
10	9.20	9.85	0.65	7.07
50	9.68	10.31	0.63	6.51
100	9.83	10.45	0.62	6.31

Table 3 Return Periods and Corresponding Significant Wave Heights based on Annual Maximum Series, NSB II.

T_R [year]	Description	H_S [m]	T_P [m]	H [m]	T [s]
50	Buoy	7.46	11.20	14.00	9.32-16.10
50	Hindcast	8.21	12.70	15.27	10.60-16.10

Table 4 Design Wave Parameter for NSB-II.

Height	Radius	Thickness	Top Mass	Abutment	Elements	Time Step
[m]	[m]	[m]	[t]	[-]	[-]	[s]
97.0	2.5-1.73	0.045	290	Clamped	99	0.2

Table 5 Properties of Monopile Model

`

Description	H[m]	T[s]	Load [kN]	Response [kN]
B1	14.00	9.32	2371.85	2757.09
B2	14.00	11.20	2264.07	2317.63
B3	14.00	13.00	2190.35	2419.07
B4	14.00	16.10	2214.78	2291.02
H1	15.26	10.60	2509.58	2837.04
H2	15.26	12.30	2501.99	3032.81
H3	15.26	14.00	2476.36	2863.90
H4	15.26	16.10	2532.28	2545.52

Table 6 Wave Parameters and Corresponding Loads for Monopile Support Structure.

H_s	T_p	N_R Cycles	Extrapolated max. Response Amplitude R
7.46 m	11.20 s	2357	2460.12kN
8.21 m	12.70 s	1815	2209.74 kN

Table 7 Observed and Extrapolated Extreme Response Amplitudes for Monopile Support Structure.

Symbol	Description	Unit
H	individual wave height	[m]
H_s	significant wave height	[m]
H_{max}	maximum individual wave height	[s]
T	wave period	[s]
T_p	peak period	[s]
T_z	mean zero crossing period	[s]
T_{Hs}	associated period for significant wave height	[s]
T_{Hmax}	associated period for maximum individual wave height	[s]

Table 8 List of Symbols.

FIGURES

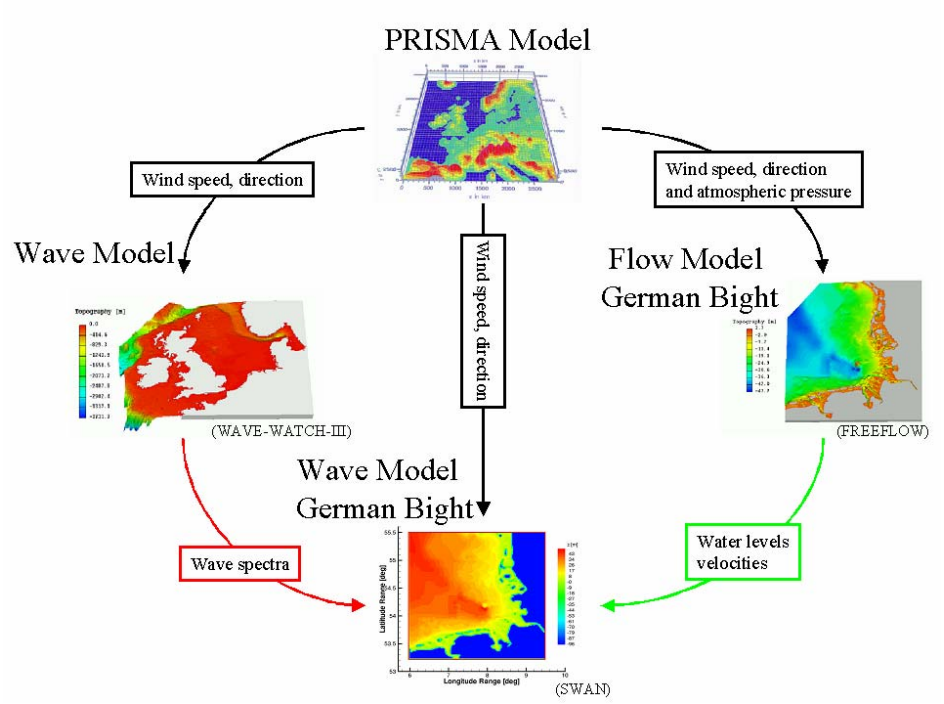

Figure 1 Coupling procedure for wave simulation.

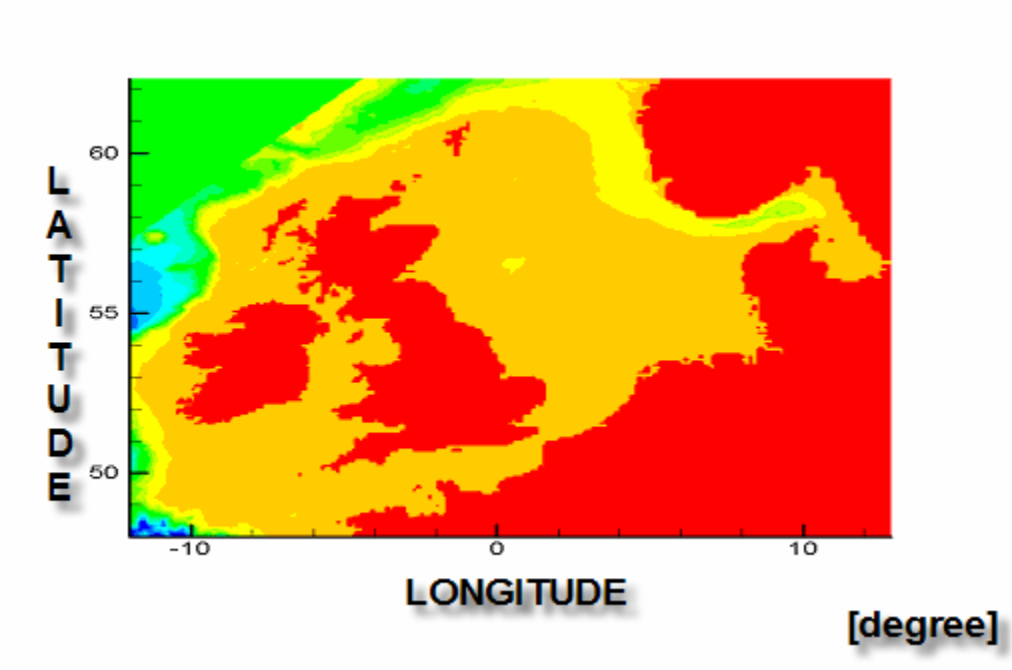

Figure 2 Domain of the European Shelf Model.

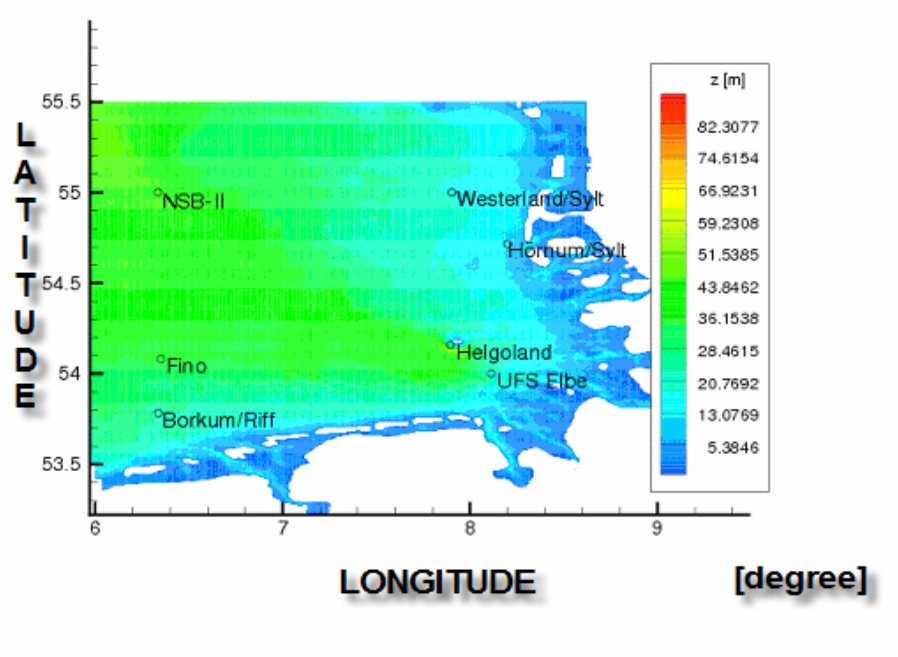

Figure 3 BSH buoys in the German Bight.

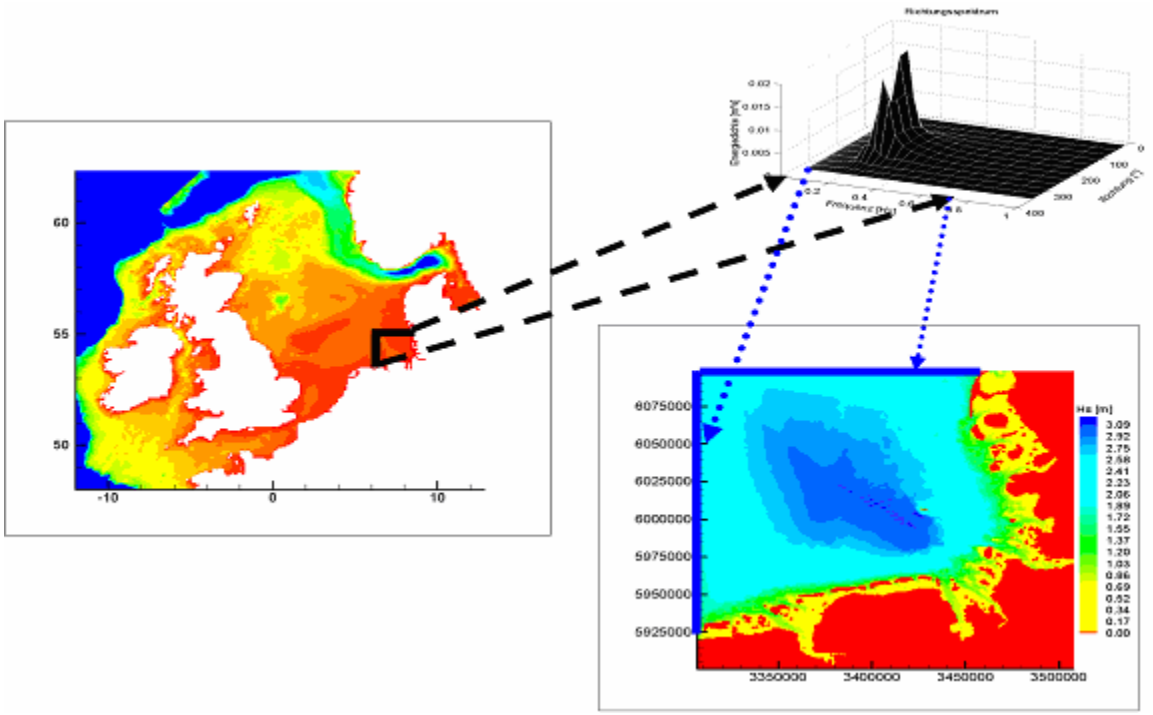

Figure 4 Procedure for coupling the European Shelf and the German Bight models.

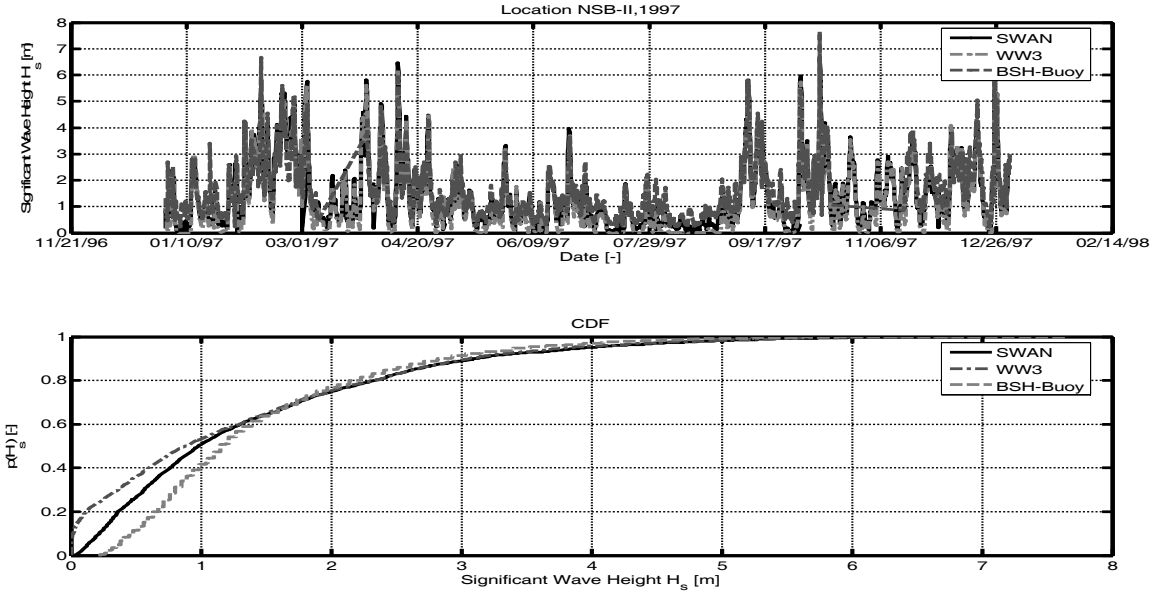

Figure 5 Comparison of Simulation and Measurement, Time History and CDF Plot of Significant Wave Heights in 1997.

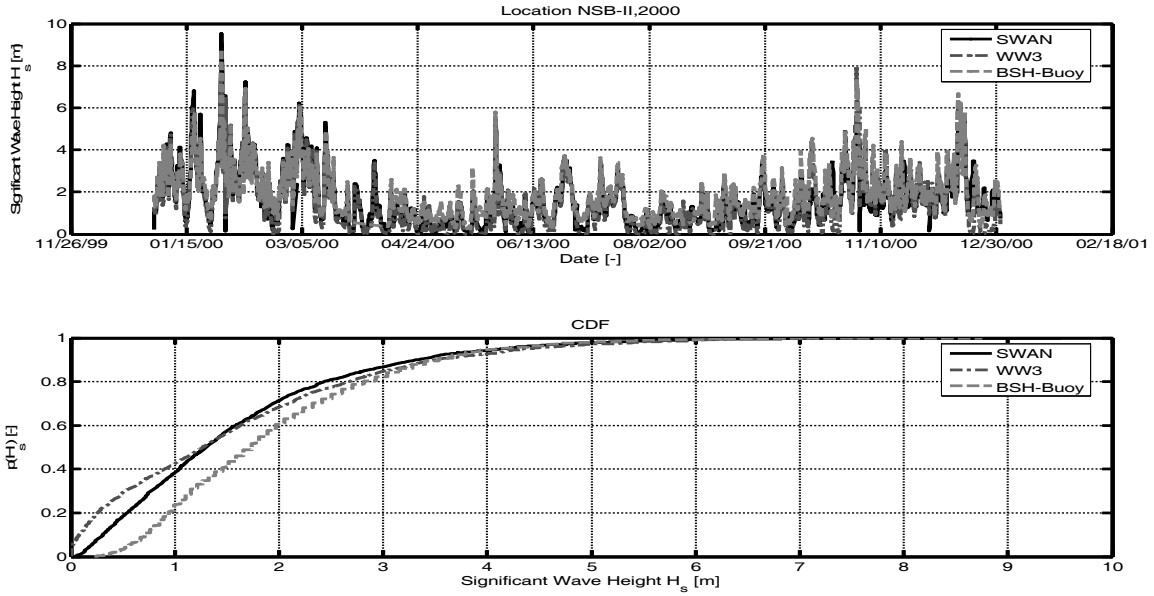

Figure 6 Comparison of Simulation and Measurement, Time History and CDF Plot of Significant Wave Heights in 2000.

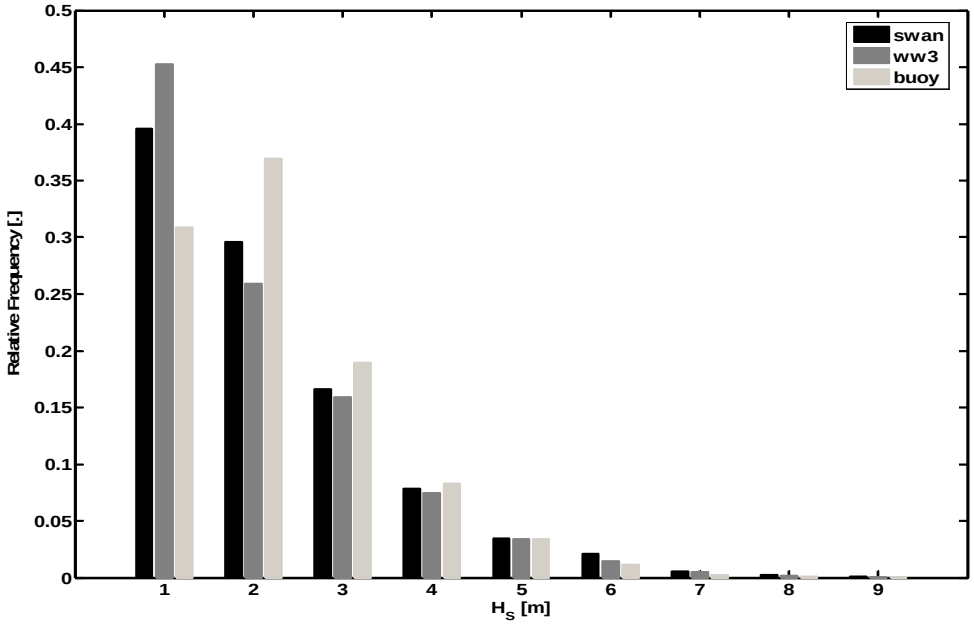

Figure 7 Relative Frequency of Occurrence of Significant Wave Heights.

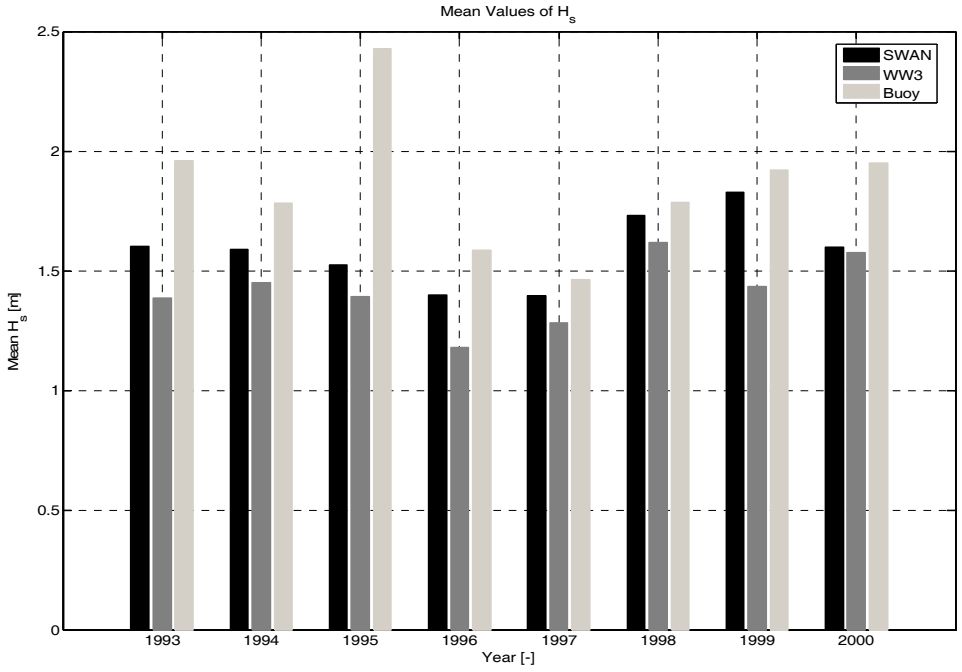

Figure 8 Annual Mean Significant Wave Heights.

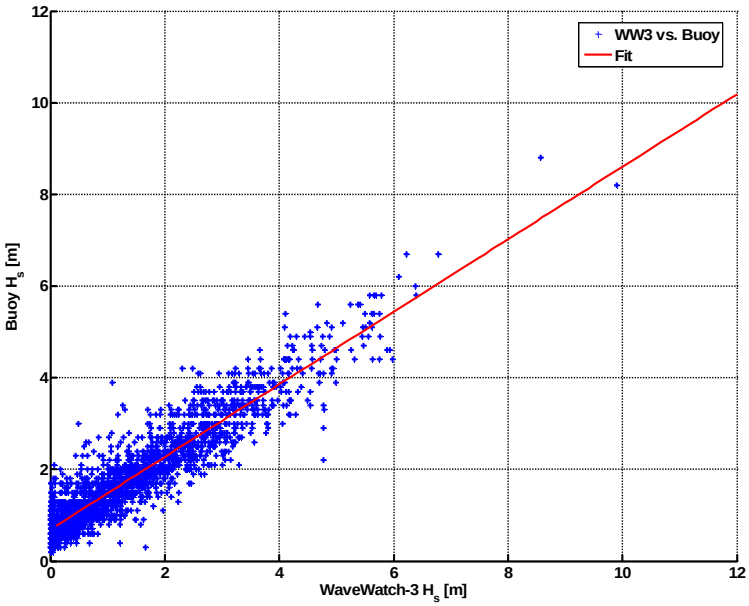

Figure 9 Scatter Plot of WaveWatch-III vs. Buoy NSB-II during 1989 to 2000.

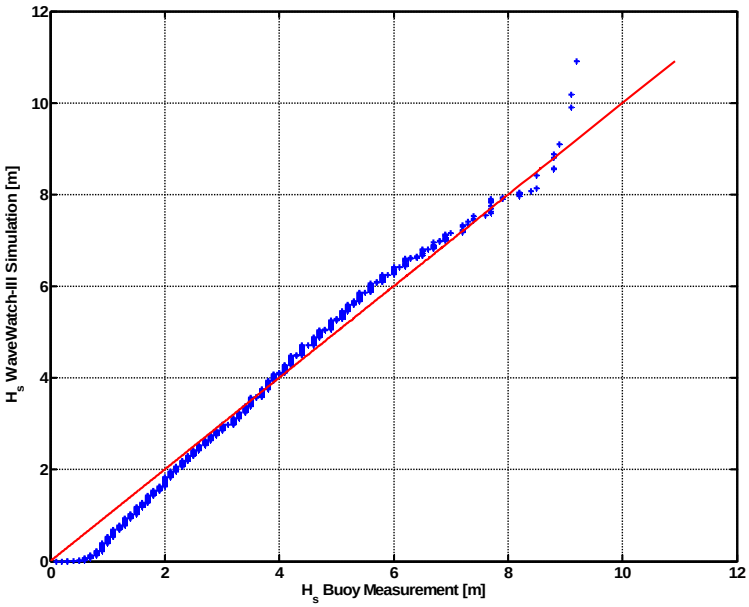

Figure 10 Quantile-Quantile Plot Buoy NSB-II vs. WaveWatch-III for the Period 1989 to 2000.

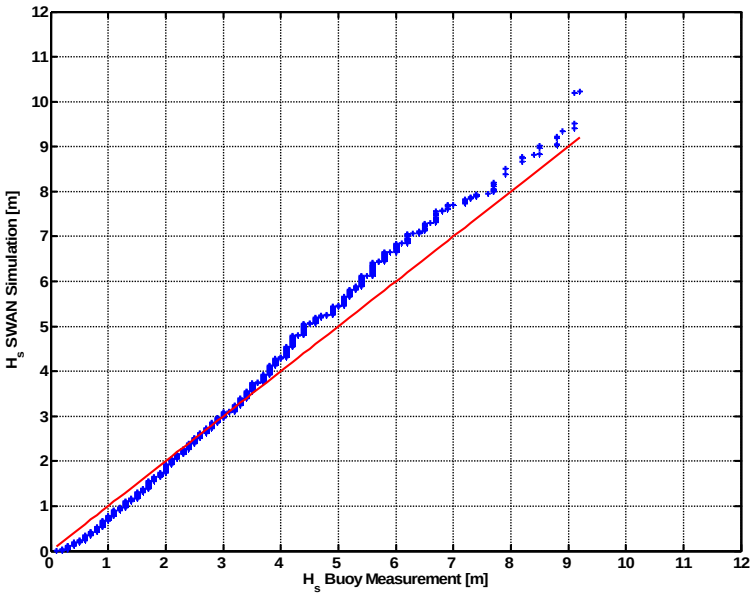

Figure 11 Quantile -Quantile Plot Buoy NSB-II vs. SWAN for the Period 1989 to 2000.

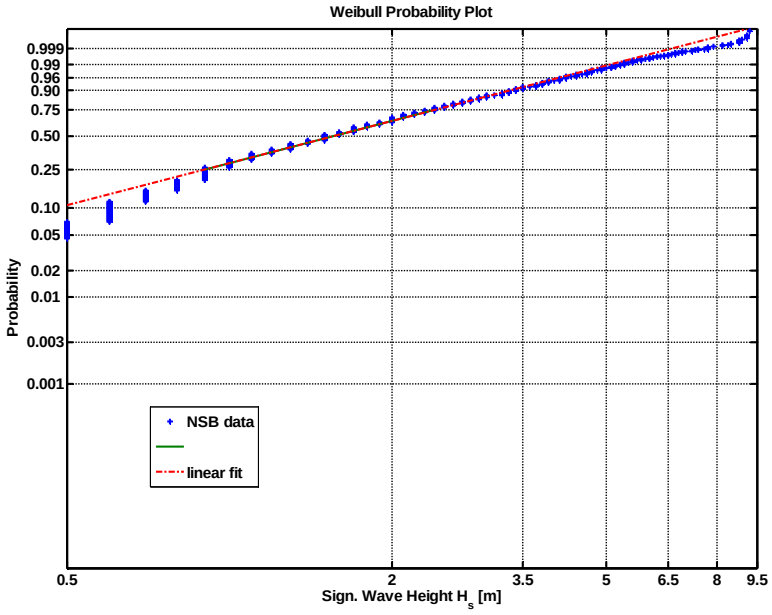

Figure 12 Weibull Plot of Measured Significant Wave Heights.

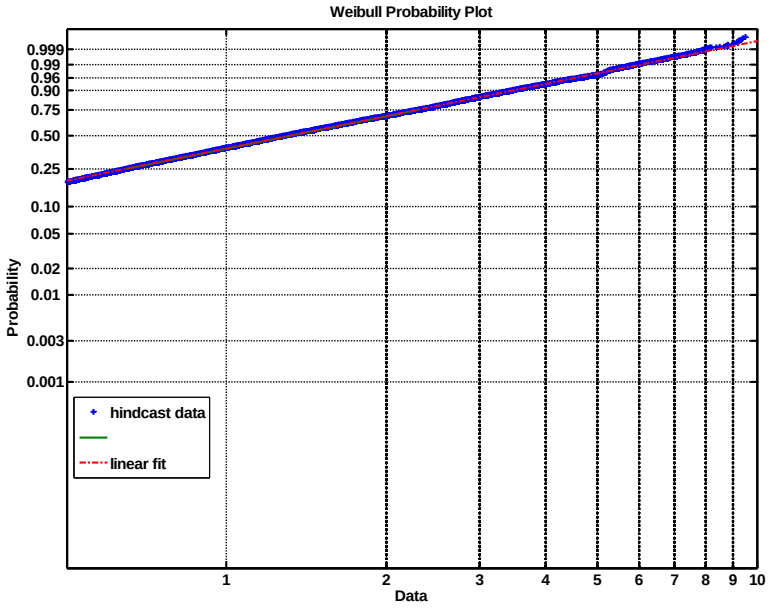

Figure 13 Weibull Fit of Simulated Significant Wave Heights (Hindcast).

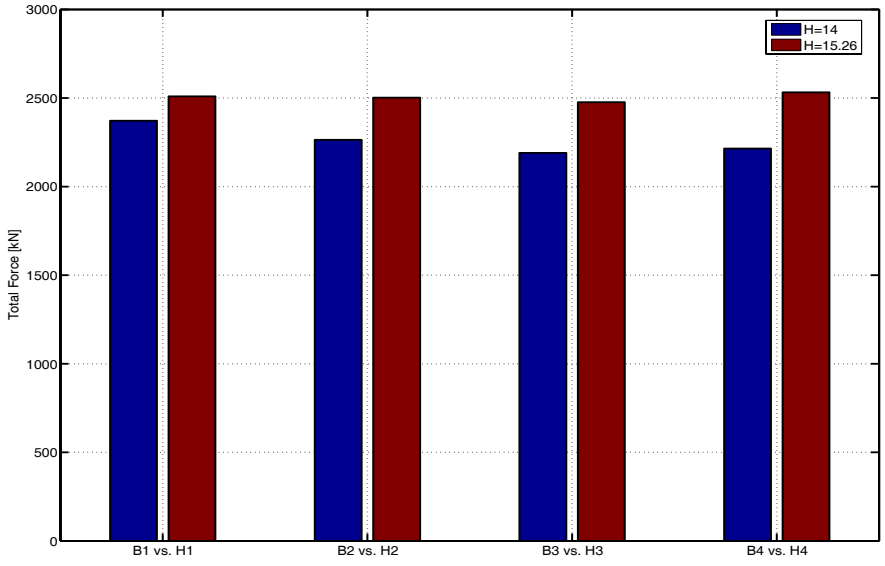

Figure 14 Total Loads due to Regular Waves with Different Wave Heights (Parameters given Table 6).

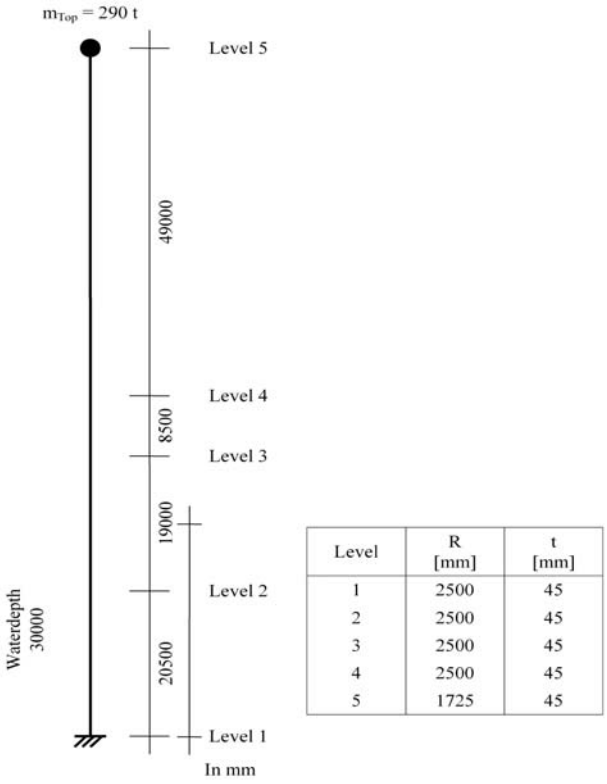

Level	R [mm]	t [mm]
1	2500	45
2	2500	45
3	2500	45
4	2500	45
5	1725	45

Figure 15 Simulation Model for Monopile Structure, R: Radius, t: Wall Thickness.

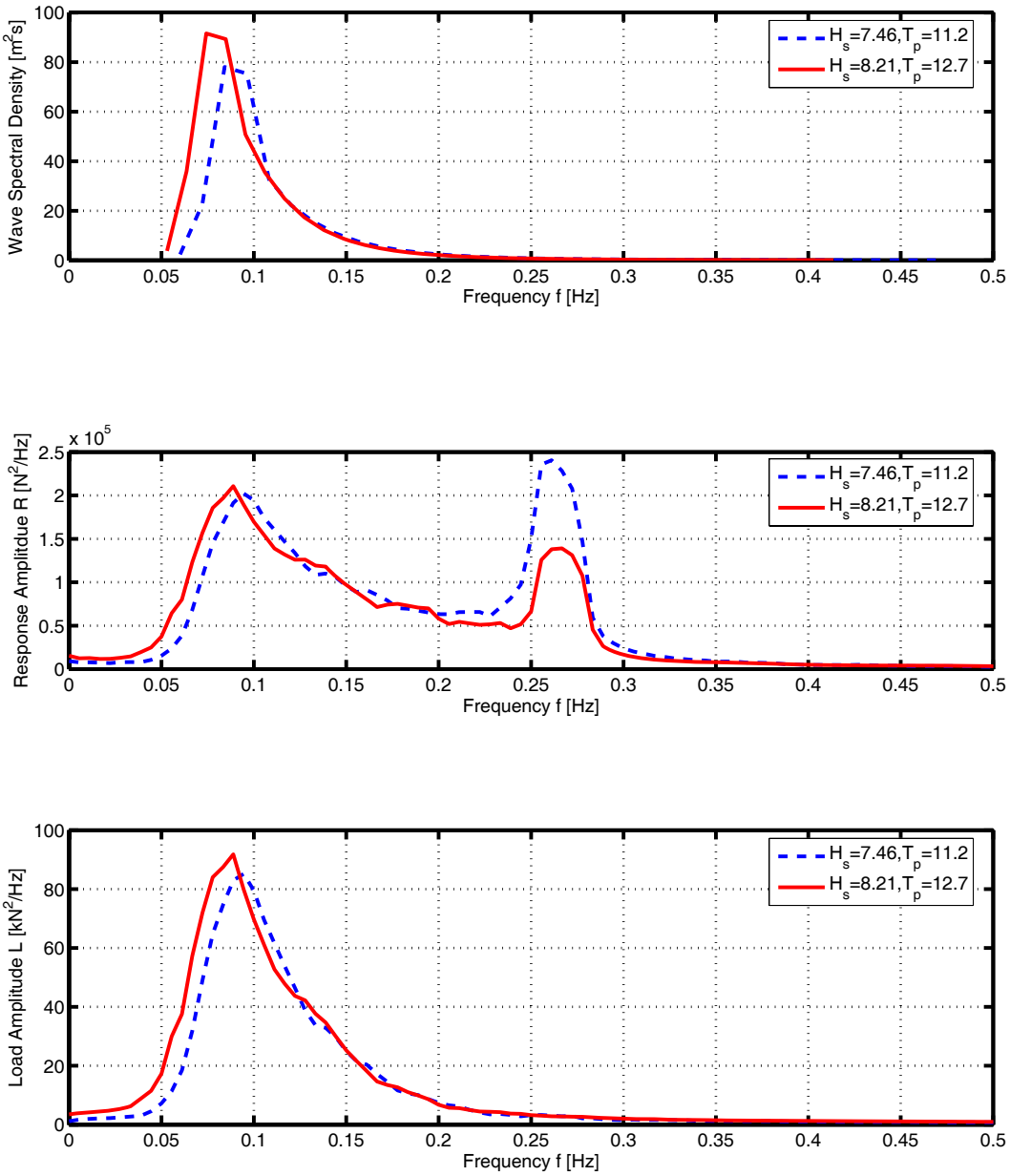

Figure 16 Wave Spectra, Response Spectra and Transfer Functions.